PROCEEDINGS OF SPIE

SPIEDigitalLibrary.org/conference-proceedings-of-spie

Optical system for enhancing the precision of geometric parameter estimation for objects utilizing defocused images

Yosyp Bilynsky, Stepan Zhivotivskyi, Alexander Nikolsky, Dmytro Baranovskyi, Olena Tsikhanovska, et al.

Yosyp Bilynsky, Stepan Zhivotivskyi, Alexander Nikolsky, Dmytro Baranovskyi, Olena Tsikhanovska, Orken Mamyrbayev, Róża Dzierżak, Aizat Kydyrbekova, "Optical system for enhancing the precision of geometric parameter estimation for objects utilizing defocused images," Proc. SPIE 12985, Optical Fibers and Their Applications 2023, 129850B (20 December 2023); doi: 10.1117/12.3023051

SPIE.

Event: Optical Fibers and Their Applications 2023, 2023, Lublin, Poland

Optical system for enhancing the precision of geometric parameter estimation for objects utilizing defocused images

Yosyp Bilynsky[a,b], Stepan Zhivotivskyi[a], Alexander Nikolsky[c], Dmytro Baranovskyi[d], Olena Tsikhanovska[e], Orken Mamyrbayev[f], Róża Dzierżak[g], Aizat Kydyrbekova[h]

[a]Vinnytsia National Technical University; [b]Vinnytsia National Agrarian University; [c]National Pirogov Memorial Medical University; [d]National Aviation University; [e]West Ukrainian National University;[f]Institute of Information and Computational Technologies CS MES RK, Almaty, Kazakhstan; [g] Lublin University of Technology, Lublin, Poland; [h]South Kazakhstan University named after M. Auezov;

ABSTRACT

Today, optical systems of subpixel measurements of geometric dimensions of objects, as well as 3D triangulation measurement systems, have gained wide application. This capability is achieved under the condition of obtaining sharp images of the investigated object. However, challenges arise when the object's image or a specific part of it becomes blurred or defocused, as some of its features lie outside the focal plane. The use of defocused images leads to significant measurement errors during their computer processing.

The paper introduces a method based on the use of two defocused images of the research object. Through advanced computer processing, this approach enables obtaining a sharp image, extracting its contour, and acquiring its geometric parameters with subpixel precision.

Keywords: depth of field, edge point, contour extraction, optical system, photo camera, scanning, image processing.

1. INTRODUCTION

Optoelectronic devices (OED) provide a unique opportunity to measure the geometric and dynamic parameters of a wide range of objects in real-time with high spatial resolution, by analyzing both their own light and the transmitted light. Typically, a charge-coupled device (CCD) serves as the photodetector in such devices. By using the pixel signal dependence of the CCD matrix on the light intensity distribution under specific conditions, the accuracy of the coordinates determining between two contrasting image areas can be enhanced.

To achieve this accuracy, it is essential to obtain the optimal depth of field (DOF), which represents the distance along the optical axis between the front and rear boundaries of the sharp image, within which the objects captured in the image appear sufficiently sharp. However, obtaining the optimal DOF for precise determination of the object's geometric parameters remains a complex task[1,2,3.]

The purpose of this study is to explore the theoretical foundation for developing a method to enhance the measurement accuracy of coordinates for a wide range of objects, especially when their images are captured with a shallow depth of field.

2. MATHEMATICAL MODEL

The blurring formed in the image due to scattering depends on the distance between the object being captured and the focal plan. The larger the diameter of such blurring, the more unsharp the object's image becomes. Points of objects located outside the focal plane can appear sharp if the diameters of the corresponding blur circles do not exceed the acceptable circle of confusion. Therefore, the depth of field (DOF) is influenced by the lens's focal length. Consequently, during the scanning of an object, there is always a certain level of measurement inaccuracy when identifying the edge points of the image. This inaccuracy is primarily associated with the magnitude of signal scattering in the optical system and the characteristics of the CCD matrix[1,4,5].

Optical Fibers and Their Applications 2023, edited by Waldemar Wójcik, Zbigniew Omiotek, Andrzej Smolarz, Proc. of SPIE Vol. 12985, 129850B · © 2023 SPIE
0277-786X · doi: 10.1117/12.3023051

It is considered that optoelectronic channels of optoelectronic systems (OES), designed for measuring the geometric parameters of objects, have a large number of optical transmission stages. Therefore, the optical transfer function (OTF) of the optical path is typically approximated by a Gaussian function. Since such an OTF lacks a phase component (i.e., it equals zero), the amplitude component of the OTF can also be described by the same Gaussian function as the OTF[2].

The central limit theorem states that the distribution of the sum of independent random variables approaches a normal (Gaussian) distribution as the number of variables becomes large and is analogous to the theory of linear filtering. In the context of optical systems, this means that the product of several spatial-frequency characteristics of individual optical elements approximates a Gaussian form when the number of elements becomes large[6]. This circumstance highlights the significance of the Gaussian function, as it provides a reasonably accurate description of the spatial-frequency properties of real optoelectronic devices[3,4,7].

The mathematical representation of the normalized Gaussian rotationally symmetric function is given by:

$$G(x,y)=\exp\left(-\frac{x^2}{2\sigma^2}\right)\cdot\exp\left(-\frac{y^2}{2\sigma^2}\right), \tag{1}$$

where σ is the standard deviation of the distribution of the intensity variation of the reflected light at the boundary (a constant in the Gaussian law).

If the optoelectronic system (OES) consists of two or several optical paths with distinct optical transfer functions or if one of the paths allows for the alteration of its transfer function, it is possible to obtain common points of adjacent image curves of objects captured by these systems in real-time with minimal computer processing efforts. Common points of adjacent image curves are typically located at the level of 0.5 normalized image curves and have the maximum value of the derivative at this point, which corresponds to the coordinate of the object's edge in the image[6].

Normalized intensity profiles, obtained in Mathcad for multiple values of optical transfer functions that share a common edge point according to formula (1), are presented in Fig. 1

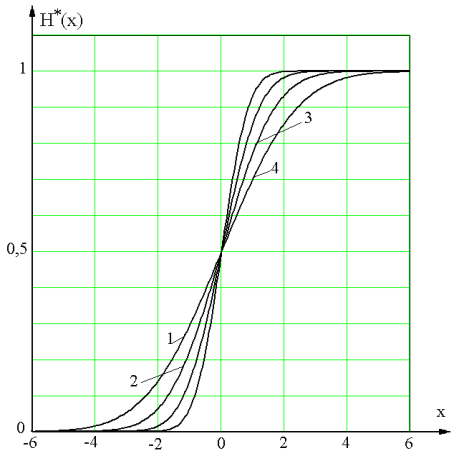

Figure 1. Before determining the intersection point of normalized intensity profiles.

The transfer characteristics of certain elements, such as CCD matrices, demonstrate that they are not spatially invariant optical transfer functions because their point spread function (PSF) has a periodic nature and equals zero only at points where the image edges coincide with the edges of the photodetectors.

Let the object have a two-dimensional intensity distribution of sharp edges[9]:

$$H(x,y)=\begin{cases}0 \text{ when } x<x_0;\\ 1 \text{ when } x>x_0;\\ \frac{1}{2} \text{ when } x_0=0;\\ \text{for every } y\end{cases} \tag{2}$$

The distribution of the signal of a sharp edge on a continuous photodetector along the x-axis is uniquely associated with it and is determined by its appearance, as shown in Fig. 2.
The intensity signal distribution in the case of a continuous photodetector is determined by the formula[10]:

$$H^*(x,y) = k \cdot H(x,y) ** O(x,y) ** P(x,y) \ , \tag{3}$$

where $O(x,y)$, $P(x,y)$ – aperture functions of the optical system and the photodetector element, respectively;
$H(x,y)$ – intensity distribution of the observed object;
K – coefficient of conversion of light energy quantities into electrical quantities.

For the discrete representation of the intensity distribution, considering the spatial non-invariance of the transfer function of the matrix receiver, model (2) is transformed into the following expression for one-dimensional space:

$$H_1^* = \frac{1}{\sqrt{2\pi\sigma}} \int_{-\infty}^{x} \exp\left[\frac{-t^2}{2\sigma^2}\right] dt \ . \tag{4}$$

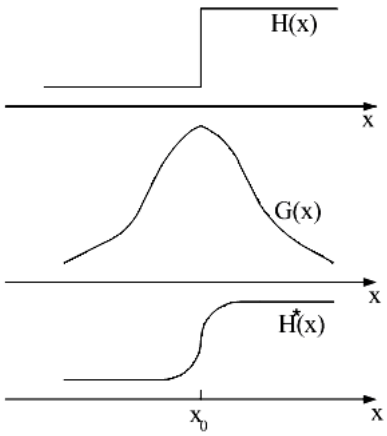

Figure 2. Appearance of the intensity distribution before and after passing through a linear optical system with a scattering function $G(x)$

After integration, we obtain:

$$H_1^* = \frac{1}{\sqrt{2\pi\sigma}} \exp - \frac{t^2}{2\sigma^2} \ , \tag{5}$$

Since the second component of the integration can be neglected, similarly, for two images with different degrees of blurring σ_1 та σ_2, we can write:

$$H_1^* = \frac{1}{\sqrt{2\pi\sigma_1}} \exp - \frac{x^2}{2\sigma_1^2} \ , \tag{6}$$

$$H_2^* = \frac{1}{\sqrt{2\pi\sigma_2}} \exp - \frac{x^2}{2\sigma_2^2} \ . \tag{7}$$

As a result of straightforward transformations of equations (6) and (7), we obtain an expression for determining the common point of intersection of adjacent image curves that have different degrees of blurring:

$$x = \sqrt{\frac{2\pi \ln \frac{H_1^x}{H_2^x}\sqrt{\frac{\sigma_1}{\sigma_2}}}{\frac{1}{\sigma_2}-\frac{1}{\sigma_1}}} \tag{8}$$

The degrees of blurring σ_1 та σ_2 can be represented, considering the intensity gradient and the width of the interpixel space, as a normalized function defined as:

$$\sigma_\partial = \frac{(I_{\max} - I_{\min})\beta d}{\Delta I\sqrt{2\pi}}, \tag{9}$$

where I_{max}– maximum intensity value; I_{min} – minimum intensity value; β– proportionality coefficient; d– width of the interpixel space.

The proportionality coefficient β corresponds to the ratio of its normalized value to the step of discretization $\frac{\Delta_{normal}}{\Delta}$.

Expression (8) allows obtaining common points of adjacent image curves from defocused images. This, in turn, enables proposing a method to enhance the sharpness of the imaged object, extract its contour, and subsequently determine its geometric parameters based on using defocused images of the object with different degrees of blurring.

3. EXPERIMENTAL SECTION

To confirm the proposed method, experimental investigations were conducted. Fig. 3 shows the experimental setup, which consists of a projector (P), a camera (C), a semi-transparent mirror (M), and a screen (A) onto which a pattern in the form of black-and-white stripes is projected.

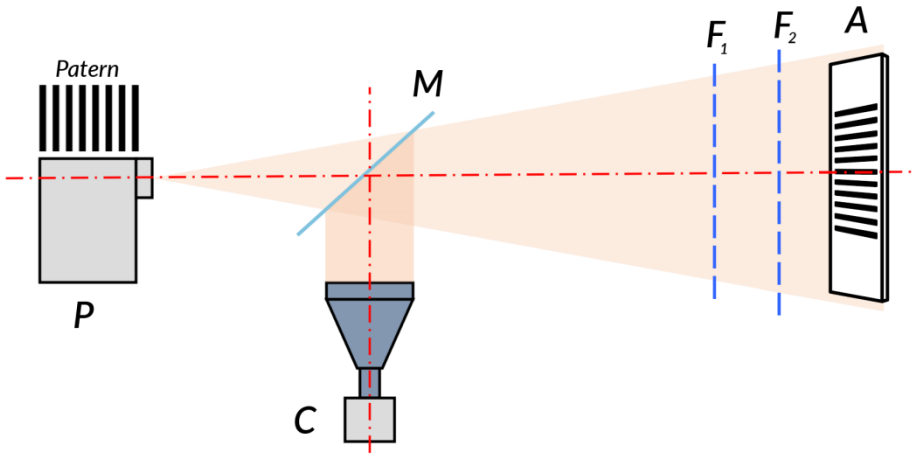

Figure 3. Experimental setup diagram

The camera (C) was set to manual focus mode, allowing us to obtain a sharp image of the pattern. By gradually changing the focal distance, two additional images of the scene with different degrees of blurring were captured. Consequently, three shots were obtained, one clear and two with varying degrees of blurring, as shown in Fig. 4.
In Fig. 5, the oscillograms of a single horizontal line of pixels obtained from the two blurred images are shown, indicating the presence of common edge points in the pattern images.

a) b) c)

Figure 4. The three captured images with different degrees of blurring.
a) Blurred image with σ_1 , b) Blurred image with σ_2, c) Focused image.

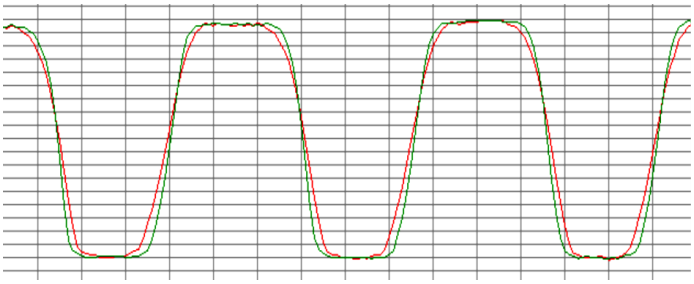

Figure 5. Oscillograms of a single horizontal line of pixels from two blurred images

To implement this function, the logical operation “AND”, is insufficient, as common points can fall on both common pixels and interpixel spaces. Therefore, the coordinates of the common edge points are determined with subpixel accuracy[11].
To confirm the adequacy of the proposed method, the contoured image was compared with the sharp image of the patterns (Fig. 4c). For this purpose, a contour image was obtained based on the focused image using the Laplacian method (Fig. 6b)[12,13].

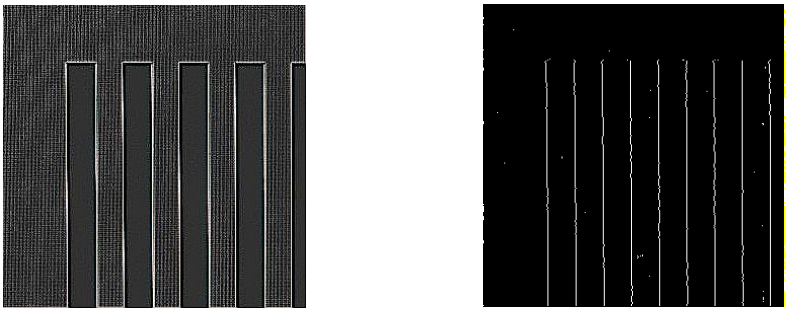

a) b)

Figure 6. Contour extraction of pattern images.
a) Contour extraction of the pattern image by finding common edge points from the intersection of blurred images.
б) Contour extraction of the sharp image using the Laplacian method.

Fig. 7 illustrates the oscillograms of a single pixel row in the contoured image obtained using the proposed approach (top) and the contoured image acquired from the sharp image using the Laplacian method (bottom)[14]

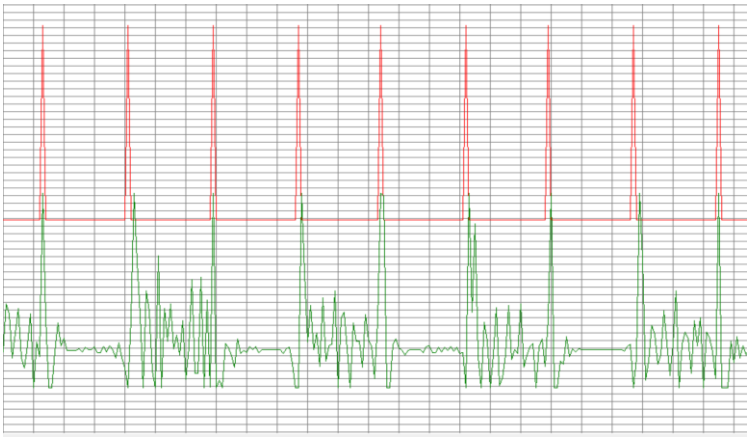

Figure 7. Oscillograms of a single pixel row in the contoured image obtained using the proposed approach (top) and the contoured image acquired from the sharp image using the Laplacian method (bottom).

Visual analysis of the oscillograms, as well as the application of filtering error criteria such as RMSE and peak signal-to-noise ratio (PSNR), indicated a high level of contour alignment, suggesting the practical viability of the proposed method.

4. CONCLUSIONS

The paper proposes a method for measuring the geometric dimensions of objects using defocused images obtained through an optoelectronic system. The proposed mathematical model for determining edge points of the object confirms the feasibility of using such a method, which involves using two defocused images of the object with different degrees of blurring. Experimental studies have been conducted, confirming the relevance and effectiveness of this approach.

REFERENCES

[1] Bozhko, K. M., Sydorenko, S. Y. and Kushchovyi, S. M. “Improvement of control of connections of optical parts with the help of television means,” Technology audit and production reserves (25), 55-59 (2015).

[2] Bilinskyi, Y.Y. “Analysis of modern multi-element photoreceiving devices and optical-electronic methods and tools based on them,” Visnyk of Vinnytsia Polytechnical Institute 5(62), 9-15 (2005).

[3] Khramov, A. V. “Primary converters of measuring devices and automatic systems: Higher school,” Materials of the conference IAMG2011, September 5-9, Salzburg, Austria, 1393-1403 (2011).

[4] Timchenko, Leonid I. , Kokriatskaia, Natalia I., and et al. "Q-processors for real-time image processing," Proc. SPIE 11581, Photonics Applications in Astronomy, Communications, Industry, and High Energy Physics Experiments, 115810F (2020).

[5] Avrunin, O. G., Nosova, Y. V., Abdelhamid, I. Y., et al. “Possibilities of automated diagnostics of odontogenic sinusitis according to the computer tomography data,” Sensors 21(4), 1-22, (2021).

[6] Fischer, J. “DSP Based Measuring Line-scan CCD Camera,” Proceedings of IDAACS, 345-348 (2003).

[7] Avrunin, O.G.; Nosova, Y.V.; Abdelhamid, I.Y.; et al. “Research Active Posterior Rhinomanometry Tomography Method for Nasal Breathing Determining Violations,” Sensors 21, 8508 (2021).

[8] Nair, D. “On comparing the performance of object recog¬nition systems,” International Conference on Image Processing, 631-634 (1995).

[9] Bilynsky, Y., et al. “Subpixel edge detection method based on low-frequency filtering,” Proc. SPIE 10031, Photonics Applications in Astronomy, Communications, Industry, and High-Energy Physics Experiments 1003152 (2016).

[10] Bilynsky, Y., Ratushny, P., Yukysh, S., Barylo, A., et al. “Contouring of microcapillary images based on sharpening to one pixel of boundary curves,” Proc. SPIE 10445, Photonics Applications in Astronomy, Communications, Industry, and High Energy Physics Experiments 104450Y (2017).

[11] Pavlov, S.V., Kozhukhar, A.T., Titkov, S.V. et al. “Electro-optical system for the automated selection of dental implants according to their colour matching,” Przeglad Elektrotechniczny 93(3), 121–124 (2017).

[12] Rovira, J. R., Pavlov, S. V., Vassilenko, V. B., Wójcik, W. et al. "Methods and resources for imaging polarimetry", Proc. SPIE 8698, Optical Fibers and Their Applications 86980T (2013).
[13] Pavlov, S.V., Kozhemiako, V.P., Petruk, V.G. and Kolesnik, P.F., "Photoplethysmohrafic technologies of the cardiovascular control," Vinnitsa: Universum-Vinnitsa, 254 (2007).
[14] Wójcik, W., Pavlov, S. and Kalimoldayev, M., "Information Technology in Medical Diagnostics II," London: Taylor & Francis Group, CRC Press, Balkema book, 336 (2019).